Effect of extended confinement on the structure of edge channels in the quantum anomalous Hall effect

Z. Yue and M. E. Raikh

Effect of extended confinement on the structure of edge channels in the quantum anomalous Hall effect

Z. Yue and M. E. Raikh

Department of Physics and Astronomy, University of Utah, Salt Lake City, UT 84112, USA

Quantum anomalous Hall (QAH) effect in the films with nontrivial band structure accompanies the ferromagnetic transition in the system of magnetic dopants. Experimentally, the QAH transition manifests itself as a jump in the dependence of longitudinal resistivity on a weak external magnetic field. Microscopically, this jump originates from the emergence of a chiral edge mode on one side of the ferromagnetic transition. We study analytically the effect of an extended confinement on the structure of the edge modes. We employ the simplest model of the extended confinement in the form of potential step next to the hard wall. It is shown that, unlike the conventional quantum Hall effect, where all edge channels are chiral, in QAH effect, a complex structure of the boundary leads to nonchiral edge modes which are present on both sides of the ferromagnetic transition. Wave functions of nonchiral modes are different above and below the transition: on the "topological" side, where the chiral edge mode is supported, nonchiral modes are "repelled" from the boundary, i.e. they are much less localized than on the "trivial" side. Thus, the disorder-induced scattering into these modes will boost the extension of the chiral edge mode. The prime experimental manifestation of nonchiral modes is that, by contributing to longitudinal resistance, they smear the QAH transition.

PACS numbers: 75.50.Pp, 75.47.-m, 73.43.-f

I. INTRODUCTION

Quantum anomalous Hall effect is achieved by doping the films possessing nontrivial band structure with magnetic impurities.[4–15,28–30] This doping gives rise to a spontaneous magnetization caused by exchange between the impurities. The most exciting consequence of this magnetization is that the associated spin splitting re-
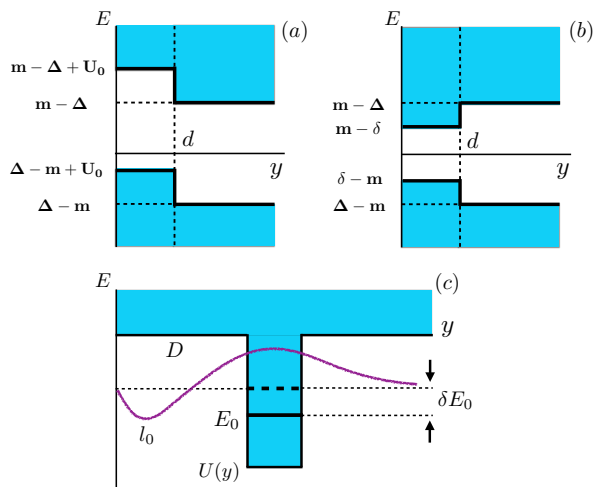

FIG. 1: (a) and (b) illustrate two variants of the extended confinement: potential step next to the hard wall (a), and step in the gapwidth next to the hard wall (b); (c) illustrates a potential well, $U(y)$, located far away from the wall (at distance $D \gg l_\Delta$). A finite-D shift, δE_0, of the guided mode, $E_0(k_x)$, depends on whether the underlying bandstructure is trivial or inverted. Such a "sensitivity" originates from the behavior of the wave function in a narrow domain, l_0, near the boundary.

sults in the band inversion. Magnetization-induced band inversion was predicted theoretically in Refs. 16, 17. First experiments[28–30] indicated that there is a jump in non-diagonal component, σ_{xy}, of the conductivity at ferromagnetic transition confirming the theoretical prediction. Very recently[11,12], upon improving the quality of the samples, a very accurate quantization of σ_{xy} was demonstrated.

In experiments[4–15,28–30], the ferromagnetism is switched on and off by application of a weak external field. The observed quantized steps in non-diagonal resistance look similar to the steps observed in conventional quantum Hall effect only in much weaker external fields. One of the conclusions which can be drawn from these experimental studies is that the structure of the edge states plays a crucial role in achieving an almost zero longitudinal resistance, ρ_{xx}.

On the theoretical side, it was demonstrated numerically in Ref. 18 that the dispersion law of the edge states in realistic multilayer QAH structure contains nonchiral edge modes along with a chiral one. It was also demonstrated in Ref. 18 that coexistence of chiral and nonchiral edge modes leads to a finite longitudinal resistance. In order to suppress the contribution of nonchiral channels to ρ_{xx}, in experiment Ref. 11 it was proposed to localize them by disorder. Indeed, for nonchiral edge modes, the backscattering and, consequently, the interference is allowed. This interference, on the other hand, is the origin of the quantum localization.

In theory, the question whether or not a given band structure allows a chiral edge state is decided by calculating the Chern number. Naturally, this calculation does not answer a question whether or not this band structure supports nonchiral in-gap edge modes. Alternative microscopic approach[19–22] to the issue of edge states confirms the prediction about their presence or absence made

on the basis of Chern number calculation. This microscopic approach also allows to calculate analytically the modification of the wave function of the chiral edge state due to the orbital action of magnetic field and, even, to trace how this edge state transforms into the quantum Hall edge state upon increasing the field. However, microscopic approach[19–22] equally does not reproduce the nonchiral modes within the envelop-function description.

The Hamiltonian describing the gapped edge spectrum in QAH has a 2×2 matrix form.[16] This is in contrast to the conventional spin-orbit 4×4 Hamiltonian[23] describing the states in HgTe-based quantum wells. The reason is that the transition between inverted and trivial band structures due to magnetization takes place only for one spin projection. As a consequence of the matrix form of the Hamiltonian, the in-gap eigenstates are characterized by two decay lengths. Edge state is allowed if the two corresponding eigenvectors can be combined to satisfy the hard-wall boundary condition.[27] It appears that only "nontrivial" band structure allows such combination.

In the present paper we demonstrate that nonchiral edge modes emerge naturally upon generalization of the microscopic approach[19–22] to the case of the extended confinement. In fact, we employ the simplest model of the extended confinement in the form of a step next to the hard wall. We demonstrate that both chiral and nonchiral modes emerge as solutions of the same characteristic equation. The wave functions of nonchiral modes oscillate within the step before decaying into the bulk. Within the simplest model considered, we compare, for the same confinement, nonchiral edge modes for inverted band structure, supporting the chiral mode, and for "trivial" band structure. Our main finding is that, for "trivial" band structure, the nonchiral modes have a lower threshold with respect to e.g. the step height. Nonchiral modes with inverted band structure are more extended. Disorder-induced scattering into these states extends the localization length of the chiral edge mode.

II. EDGE MODES IN THE PRESENCE OF A STEP

A. Hard wall

To introduce notations, we briefly review the structure of the bulk QAH Hamiltonian[17]. It emerges from the conventional 4×4 Hamiltonian[23]

$$\hat{H}_{\text{eff}} = \begin{pmatrix} \hat{h}(\mathbf{k}) & 0 \\ 0 & \hat{h}^*(-\mathbf{k}) \end{pmatrix} \tag{1}$$

where $\hat{h}(\mathbf{k})$ is a 2×2 matrix defined as $\hat{h}(\mathbf{k}) = A(k_x\sigma_x + k_y\sigma_y) + (m + Bk^2)\sigma_z$, while σ_y, σ_z are the Pauli matrices acting in the pseudospin (electron-heavy hole) subspace.
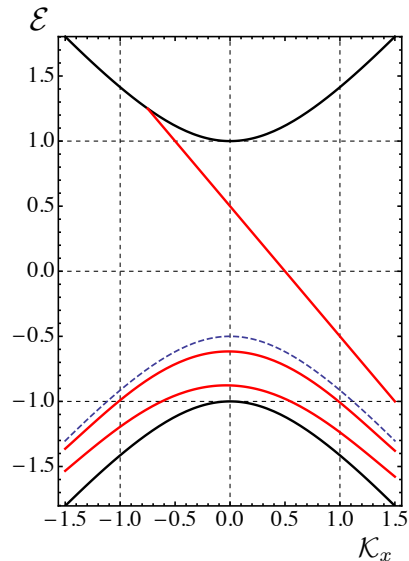

FIG. 2: (Color online) The dispersions of the modes propagating along the boundary $y = 0$ is plotted from Eqs. (18) and (22) for dimensionless step height $\tilde{U}_0 = 0.5$ and dimensionless step width $\tilde{d} = 6$. The spectrum of the edge mode and of two nonchiral modes is shown with red lines. Bulk spectrum (black) and the spectrum in the step region, $0 < y < d$, (dashed) are also shown.

Upon adding the exchange[24]

$$\hat{h}_{\text{exch}} = \begin{pmatrix} \Delta & 0 & 0 & 0 \\ 0 & -\Delta & 0 & 0 \\ 0 & 0 & -\Delta & 0 \\ 0 & 0 & 0 & \Delta \end{pmatrix} \tag{2}$$

the two blocks become inequivalent

$$\hat{h}(\mathbf{k}) \to \begin{pmatrix} m + \Delta + Bk^2 & -A(k_x - ik_y) \\ -A(k_x + ik_y) & -m - \Delta - Bk^2 \end{pmatrix} \tag{3}$$

$$\hat{h}^*(-\mathbf{k}) \to \begin{pmatrix} m - \Delta + Bk^2 & A(k_x + ik_y) \\ A(k_x - ik_y) & -m + \Delta - Bk^2 \end{pmatrix}. \tag{4}$$

Near $m = \Delta$ the band inversion takes place only in the second block. Thus the transition can be swept through by applying a weak magnetic field, since the field controls the parameter, Δ.

It follows from Eq. (4) that at the transition $m = \Delta$ the Hamiltonian possesses only a single spatial scale,

$$l_0 = \frac{B}{A}. \tag{5}$$

Away from the transition, a new spatial scale,

$$l_\Delta = \frac{A}{m - \Delta}, \tag{6}$$

appears. The theory is greatly simplified by the fact that the first scale is much smaller than the second one.[25] In
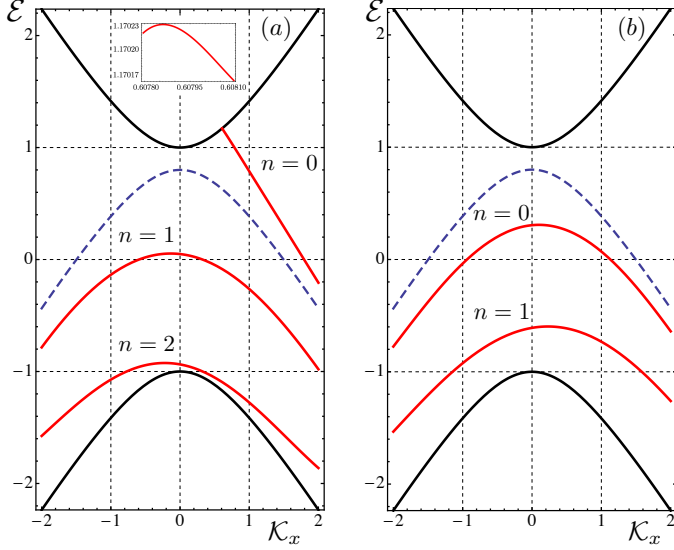
FIG. 3: (Color online) Comparison of the dispersions of edge modes, shown with red, for "topological" (a) and "trivial" (b) boundaries. Parameters of the step are $\tilde{U}_0 = 1.8$ and $\tilde{d} = 2.2$. Bulk spectrum (black) and the spectrum in the step region, $0 < y < d$, (dashed) are also shown. The inset detalizes how the dispersion of the chiral mode merges with the bulk spectrum.

terms of the edge states, for a given, say positive, sign of B, the edge state is present for $m < \Delta$ and is absent for $m > \Delta$. To see this, consider the two eigenvectors of $\hat{h}^*(-\mathbf{k})$ propagating, as $\exp(ik_x x)$, along the boundary $y = 0$ and decaying, as $\exp(-qy)$, into the bulk, $y > 0$. For these eigenvectors, the elements of corresponding pseudospinors are related as

$$[m - \Delta + B(k_x^2 - q^2) - E]\alpha + A(k_x - q)\beta = 0,$$
$$[m - \Delta + B(k_x^2 - q^2) + E]\beta - A(k_x + q)\alpha = 0. \quad (7)$$

With $l_0 \ll |l_\Delta|$, the q-values for the two eigenvectors differ strongly, and the expressions for them have a simple form

$$q_0 = \frac{1}{l_0}, \quad q_\Delta = \frac{1}{|l_\Delta|}\sqrt{1 + (l_\Delta k_x)^2 - \left(\frac{El_\Delta}{A}\right)^2}. \quad (8)$$

Note that, by virtue of the condition $l_0 \ll |l_\Delta|$, the nonparabolicity parameter B does not enter into q_Δ. Substituting Eq. (8) into Eq. (7), we find the form of the corresponding eigenvectors

$$\Psi_0 = \begin{pmatrix} -1 \\ 1 \end{pmatrix} \exp\left[ik_x x - q_0 y\right], \quad (9)$$

$$\Psi_\Delta = \begin{pmatrix} 1 \\ \frac{A(k_x + q_\Delta)}{m - \Delta + E} \end{pmatrix} \exp\left[ik_x x - q_\Delta y\right]. \quad (10)$$

To satisfy the hard-wall boundary condition, both components of the linear combination of the eigenvectors Eqs.
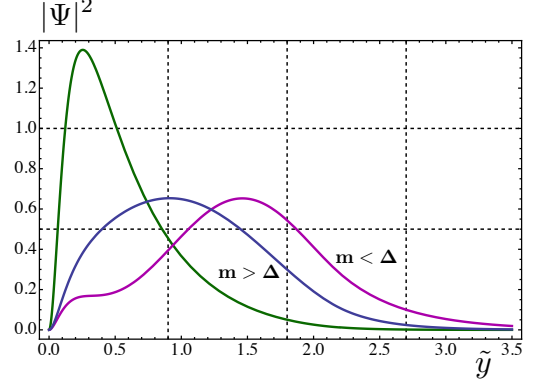

FIG. 4: (Color online) Comparison of the probability density profiles for different edge modes. For "topological" boundary the profiles of chiral edge mode and lowest nonchiral mode are shown with green and purple, respectively. The profile for the nonchiral mode at "trivial" boundary is shown with blue. All three profiles are calculated for energy in the center of the gap.

(9), (10) should turn to zero at $y = 0$. This amounts to the requirement

$$1 + \frac{A(k_x + q_\Delta)}{m - \Delta + E} = \frac{2(Ak_x + E)}{m - \Delta + E + A(k_x - q_\Delta)} = 0. \quad (11)$$

One immediately concludes from Eq. (11) that the dispersion law of the chiral edge mode is linear

$$E = -Ak_x. \quad (12)$$

However, this conclusion applies only on one side of the transition, namely, for $(m - \Delta) < 0$. Indeed, as it follows from Eq. (8), for $E = -Ak_x$, we have $q_\Delta = A/|m - \Delta|$. Therefore, for positive $m - \Delta$, the denominator in Eq. (11) turns to zero together with the numerator, so that the boundary condition cannot be satisfied.

B. Chiral edge mode in the presence of a step

Consider a boundary with a potential step next to it depicted in Fig. 1. In the domain $0 < y < d$ the potential is equal to U_0. It creates the energy shift, so that the value q_Δ gets modified

$$q_\Delta \to \kappa = \frac{1}{|l_\Delta|}\sqrt{1 + (l_\Delta k_x)^2 - \left[\frac{(E - U_0)l_\Delta}{A}\right]^2}. \quad (13)$$

A general solution within the domain $0 < y < d$ contains two growing and two decaying exponents

$$\Psi_{y<d} = C_0 \begin{pmatrix} -1 \\ 1 \end{pmatrix} \exp\left[ik_x x - q_0 y\right] + C_\Delta \begin{pmatrix} 1 \\ \frac{A(k_x+\kappa)}{m-\Delta+E-U_0} \end{pmatrix} \exp\left[ik_x x - \kappa y\right] +$$

$$D_0 \begin{pmatrix} 1 \\ 1 \end{pmatrix} \exp\left[ik_x x + q_0(y-d)\right] + D_\Delta \begin{pmatrix} 1 \\ \frac{A(k_x-\kappa)}{m-\Delta+E-U_0} \end{pmatrix} \exp\left[ik_x x + \kappa y\right]. \tag{14}$$

On the other hand, the solution for $y > d$ is still a linear combination of Ψ_0 and Ψ_Δ, namely

$$\Psi_{y>d} = C_0^- \begin{pmatrix} -1 \\ 1 \end{pmatrix} \exp\left[ik_x x - q_0(y-d)\right] + C_\Delta^- \begin{pmatrix} 1 \\ \frac{A(k_x+q_\Delta)}{m-\Delta+E} \end{pmatrix} \exp\left[ik_x x - q_\Delta(y-d)\right]. \tag{15}$$

Overall, there are 6 unknown amplitudes in Eqs. (14), (15). The 6 boundary conditions to be satisfied is vanishing of both components of the wave function at $y = 0$ and continuity of both components together with their derivatives at $y = d$. At this point we note that the step affects the dispersion law of the edge state only for $d \gtrsim l_\Delta \gg l_0$. This observation allows for two fundamental simplifications. Firstly, the term with amplitude C_0 in Eq. (14) decays rapidly with y from $y = 0$, so that its magnitude at the boundary $y = d$ is $\sim \exp(-d/l_0)$. Thus, this term should be taken into account only at the boundary $y = 0$. Similarly, the term with coefficient D_0 should be taken into account only at $y = d$. Next, the solutions with coefficients D_0 and C_0^- have big derivatives, $1/l_0$. Then, the matching with the derivatives of a slow decaying solutions, renders their amplitude small, $\sim l_0/l_\Delta \ll 1$. Neglecting the terms D_0 and C_0^- leaves us with the system for 4 unknowns with 4 boundary conditions to satisfy. The form of this system is the following

$$- C_0 + C_\Delta + D_\Delta = 0,$$
$$C_0 + C_\Delta \frac{A(k_x + \kappa)}{m - \Delta + E - U_0} + D_\Delta \frac{A(k_x - \kappa)}{m - \Delta + E - U_0} = 0,$$
$$C_\Delta e^{-\kappa d} + D_\Delta e^{\kappa d} = C_\Delta^-,$$
$$\frac{C_\Delta(k_x + \kappa)e^{-\kappa d} + D_\Delta(k_x - \kappa)e^{\kappa d}}{m - \Delta + E - U_0} = C_\Delta^- \frac{(k_x + q_\Delta)}{m - \Delta + E}. \tag{16}$$

The first two equations ensure that the wave function Eq. (14) turns to zero at $y = 0$ while the second two equations express the continuity of the wave function at $y = d$.

The consistency condition for the system Eq. (16) yields the following transcendental equation for the dispersion, $E(k_x)$, of the edge modes

$$\frac{\frac{m-\Delta+E-U_0}{A(k_x-\kappa)} + 1}{\frac{m-\Delta+E-U_0}{A(k_x+\kappa)} + 1} e^{-2\kappa d} = \frac{\frac{(k_x+q_\Delta)(m-\Delta+E-U_0)}{(k_x-\kappa)(m-\Delta+E)} - 1}{\frac{(k_x+q_\Delta)(m-\Delta+E-U_0)}{(k_x+\kappa)(m-\Delta+E)} - 1}. \tag{17}$$

To analyze this equation we first rewrite it in a dimensionless form

$$\frac{\frac{1+\mathcal{E}-\tilde{U}_0}{\mathcal{K}_x-\text{sign}(m-\Delta)\mathcal{P}} + 1}{\frac{1+\mathcal{E}-\tilde{U}_0}{\mathcal{K}_x+\text{sign}(m-\Delta)\mathcal{P}} + 1} e^{-2\mathcal{P}\tilde{d}} = \frac{\frac{[\mathcal{K}_x+\text{sign}(m-\Delta)\mathcal{Q}_\Delta](1+\mathcal{E}-\tilde{U}_0)}{[\mathcal{K}_x-\text{sign}(m-\Delta)\mathcal{P}](1+\mathcal{E})} - 1}{\frac{[\mathcal{K}_x+\text{sign}(m-\Delta)\mathcal{Q}_\Delta](1+\mathcal{E}-\tilde{U}_0)}{[\mathcal{K}_x+\text{sign}(m-\Delta)\mathcal{P}](1+\mathcal{E})} - 1}, \tag{18}$$

where we have introduced the dimensionless energy, momentum, and the decay constant

$$\mathcal{E} = \frac{E}{m - \Delta}, \quad \mathcal{K}_x = \frac{Ak_x}{m - \Delta},$$
$$\mathcal{P} = \frac{A\kappa}{|m - \Delta|} = \sqrt{1 + \mathcal{K}_x^2 - (\mathcal{E} - \tilde{U}_0)^2},$$
$$\mathcal{Q}_\Delta = \frac{Aq_\Delta}{|m - \Delta|} = \sqrt{1 + \mathcal{K}_x^2 - \mathcal{E}^2}, \tag{19}$$

while the dimensionless size and the depth of the step are defined as

$$\tilde{U}_0 = \frac{U_0}{m - \Delta}, \quad \tilde{d} = \frac{|m - \Delta|d}{A}. \tag{20}$$

Note that the sign of $(m - \Delta)$ appears in Eq. (18) to ensure that the decay constant is positive for any sign of $(m - \Delta)$.

The dispersion law Eq. (12) for the chiral edge state follows from Eq. (18) in the limit $\tilde{d} \to 0$. Indeed, in

dimensionless units, Eq. (12) reads $\mathcal{E} = -\mathcal{K}_x$. This suggests that $\mathcal{Q}_\Delta = 1$. For $(m - \Delta) < 0$, the ratio $(1 + \mathcal{E})/(\mathcal{K}_x + \text{sign}(m - \Delta)\mathcal{Q}_\Delta)$ is equal to -1, the fractions in the left-hand side and in the right-hand side are equal to each other, so that Eq. (18) is satisfied. It is even easier to see that in the limit $\tilde{d} \to \infty$ Eq. (18) yields the dispersion law $\mathcal{E} = -\mathcal{K}_x + \tilde{U}_0$. In this limit the denominator in the left-hand side turns to zero for negative $(m - \Delta)$.

For general parameters of the step the dispersion law of the chiral mode is illustrated in Figs. 2, 3. Naturally, presence of the step does not violate the fact that the chiral mode exists only for negative $(m - \Delta)$. For a "weak" step the edge mode is present for both positive and negative momenta, while for a "strong" step only at positive momenta. Although it is not a rigorous statement, the dispersion is linear with very high accuracy. Numerically, the relative change of the slope with $\mathcal{K}_x$ is $\approx 10^{-3}$.

Figs. 2, 3 also suggest that the dispersion of a chiral edge mode has an endpoint. This is also the consequence of a finite accuracy of the numerical procedure. The true behavior of the slope, as the edge mode merges with continuum at certain point $\mathcal{K}_x = \mathcal{K}_x^c$, $\mathcal{E} = \mathcal{E}^c = \left[1 + (\mathcal{K}_x^c)^2\right]^{1/2}$ is $\left[\frac{\partial\mathcal{E}}{\partial\mathcal{K}_x} - \frac{\mathcal{K}_x^c}{\mathcal{E}^c}\right] \propto (\mathcal{K}_x - \mathcal{K}_x^c)$. To see this, one can view the transcendental equation Eq. (18) as a relation between the variables $\mathcal{K}_x$ and $\mathcal{Q}_\Delta$. Since it contains the terms linear in $\mathcal{K}_x$ and $\mathcal{Q}_\Delta$, its variation yields $\delta\mathcal{K}_x = \eta\delta\mathcal{Q}_\Delta$, where η is some constant. On the other hand, from definition of $\mathcal{Q}_\Delta$ it follows that $\mathcal{Q}_\Delta\delta\mathcal{Q}_\Delta = \mathcal{K}_x\delta\mathcal{K}_x - \mathcal{E}\delta\mathcal{E}$. Thus, one has

$$\frac{\mathcal{Q}_\Delta}{\mathcal{E}} = \eta\left(\frac{\mathcal{K}_x}{\mathcal{E}} - \frac{\partial\mathcal{E}}{\partial\mathcal{K}_x}\right). \tag{21}$$

As the dispersion law approaches the continuum, the variable $\mathcal{Q}_\Delta$ turns to zero. Then it follows from Eq. (21) that the velocity of the edge mode approaches $\frac{\mathcal{K}_x^c}{\mathcal{E}^c}$, which is the velocity of the bulk mode. Numerically, the merging of the chiral edge mode dispersion with the bulk spectrum is illustrated in Fig. 3, inset. It is seen that the change of sign of the slope takes place within a very narrow domain of momenta $\sim 10^{-4}$.

C. Nonchiral edge modes

Our main finding in the present paper is that the transcendental equation Eq. (18) captures, along with the chiral mode, a set of nonchiral edge modes. For these modes the decay rate, κ, within the step and, thus, the dimensionless $\mathcal{P}$ are purely imaginary. For such $\mathcal{P}$ it is convenient to cast Eq. (18) in the form

$$|\mathcal{P}|\tilde{d} + \Phi_1 + \Phi_2 = \pi n, \tag{22}$$

where n is integer and the phases Φ_1, Φ_2 are defined as

$$\Phi_1 = \arctan\left(\frac{\text{sign}(m - \Delta)|\mathcal{P}|}{1 + \mathcal{E} - \tilde{U}_0 + \mathcal{K}_x}\right),$$

$$\Phi_2 = \arctan\left(\frac{\text{sign}(m - \Delta)|\mathcal{P}|}{\frac{1 + \mathcal{E} - \tilde{U}_0}{1 + \mathcal{E}}(\mathcal{K}_x + \text{sign}(m - \Delta)\mathcal{Q}_\Delta) - \mathcal{K}_x}\right). \tag{23}$$

The meaning of $|\mathcal{P}|\tilde{d}$ is the phase accumulated by the components of the pseudospinor on the interval $0 < y < d$, where they oscillate. The meaning of Φ_1 and Φ_2 is the phase shift at the boundary $y = 0$ and $y = d$, respectively.

The maximal value of n, i.e. the number of modes with dispersion law having its origin in the bulk gap, is finite[26] and is determined by the thickness, d.

Note that both phase shifts depend on sign of $(m - \Delta)$. Thus, the dispersion laws of nonchiral modes "know" whether or not the band structure is inverted. These dispersion laws, obtained from Eq. (22) are shown in Fig. 3 for a given step and with opposite signs of $(m - \Delta)$. It is seen that for $(m - \Delta) > 0$ the nonchiral branches lie *deeper in the gap* than nonchiral branches for negative $(m - \Delta)$. The sign of $(m - \Delta)$ also determines the classification of the branches. For $(m - \Delta) > 0$ the values of n start from $n = 0$, while $(m - \Delta) > 0$ they start from $n = 1$. Qualitatively, this suggests that a chiral mode "complicates" the formation of nonchiral modes. Different dispersions for positive and negative $(m - \Delta)$ implies that the behavior of $|\Psi(y)|^2$ is different. This is illustrated in Fig. 4. We see that nonchiral mode for $(m - \Delta) < 0$ is significantly more extended than for $(m - \Delta) > 0$.

It is instructive to compare the above results for the step potential with dispersion of nonchiral modes emerging from a jump of the gap magnitude next to the boundary in the domain $0 < y < d$, see Fig. 1b. Modifications of Eq. (18) to this case are straightforward. Firstly, the decay constant $\mathcal{P}$ should be redefined

$$\mathcal{P} \to \sqrt{\tilde{\delta}^2 + \mathcal{K}_x^2 - \mathcal{E}^2}, \tag{24}$$

where $\tilde{\delta} = (m - \delta)/(m - \Delta)$ is the relative reduction of the gap in the domain $0 < y < d$. The second modification is the replacement of the combination $1 - \tilde{U}_0$ in Eq. (18) by $\tilde{\delta}$. The solutions of Eq. (18) for a particular set of parameters are shown in Fig. 5a. Naturally, nonchiral modes are symmetric with respect to $E = 0$. Unlike the case of potential step, they never reach the midgap. With regard to the density profile, Fig. 5b, the nonchiral mode is repelled from the boundary even further than in the case of potential step.
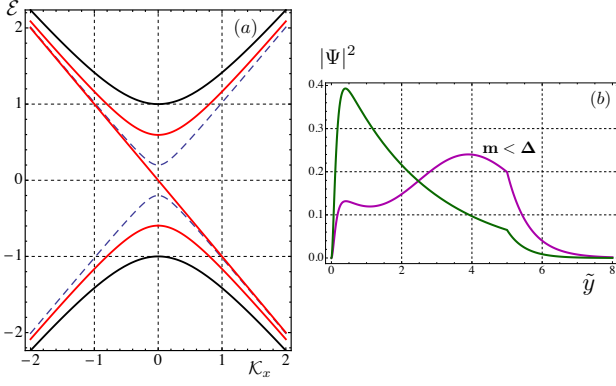
FIG. 5: (Color online) Dispersions (a) and the density profiles (b) of a chiral and nonchiral modes are shown for the extended confinement Fig. 1b. The magnitude of the gap reduction near the edge is $\delta = 0.2\Delta$, while the dimensionless width is $\tilde{d} = 5$. Density profile of both modes is calculated for dimensionless energy $\mathcal{E} = 0.6$. Bulk spectrum (black) and the spectrum in the step region (dashed) are also shown.

III. "TOPOLOGICAL" SHIFT OF THE DISPERSION OF THE MODE LOCALIZED FAR AWAY FROM THE BOUNDARY

A. Formulation of the problem

In the present Section we consider the following problem. Suppose that a potential well, $U(y)$, is located far away from the boundary, see Fig. 1c. Quantitatively,

this implies that the distance, D, is much bigger than l_Δ. Even in the limit $D \to \infty$ the potential $U(y)$ supports a nonchiral mode with dispersion, $E_0(k_x)$. This dispersion does not depend on whether the underlying band structure is trivial or inverted. Finite D causes a small correction, $\delta E_0(k_x)$, to the dispersion of the mode guided by $U(y)$. We will demonstrate that this correction has a "topological" character: it shifts $E_0(k_x)$ towards the center of the gap for $(m - \Delta) > 0$ and away from the midgap for $(m - \Delta) < 0$. Moreover, we will see that the "topological" character of the correction manifests itself in the fact that it depends on the *sign* of k_x, while the bare dispersion, $E_0(k_x)$, is obviously an even function of k_x. Qualitatively, this effect can be understood as follows. Consider the situation $(m - \Delta) < 0$. The guided mode "senses" the boundary via the far tail of the wave function, see Fig. 1c. For $(m - \Delta) < 0$ there is a chiral mode propagation along the boundary. The coupling of the tail to this mode is either strong or weak depending on weather the guided mode co-propagates ($k_x < 0$) or counter-propagates ($k_x > 0$) with the chiral mode. In the next subsection we trace analytically the resonance between the guided mode in potential $U(y)$ and the chiral edge mode. Calculation can be performed explicitly due to the small parameter l_Δ/D.

B. Calculation of the shift

Denote with $\psi_e(y)$ and $\psi_h(y)$ the components of pseudospinor describing the wave function of a nonchiral mode

$$\left(\hat{h}^*(-\hat{\mathbf{k}}) + U(y)\right)\Psi = \left(\hat{h}^*(-\hat{\mathbf{k}}) + U(y)\right)\begin{pmatrix}\psi_e\\\psi_h\end{pmatrix} = E(k_x)\begin{pmatrix}\psi_e\\\psi_h\end{pmatrix}. \tag{25}$$

For $l_0 \ll l_\Delta$ presence of the boundary is taken into account by imposing a boundary condition

$$\Psi(0) = \begin{pmatrix}1\\-1\end{pmatrix}. \tag{26}$$

We emphasize that, as in the case of a step, the meaning of $y = 0$ in this condition is, in fact, $l_0 \ll y \ll l_\Delta$, see Eqs. (9), (10). Denote now with $\psi_e^{(0)}(y)$, $\psi_h^{(0)}(y)$ the component of pseudospinor for the case when the boundary is absent (moved to $y = -\infty$). One has

$$\left(\hat{h}^*(-\hat{\mathbf{k}}) + U(y)\right)\Psi^{(0)} = \left(\hat{h}^*(-\hat{\mathbf{k}}) + U(y)\right)\begin{pmatrix}\psi_e^{(0)}\\\psi_h^{(0)}\end{pmatrix} = E_0(k_x)\begin{pmatrix}\psi_e^{(0)}\\\psi_h^{(0)}\end{pmatrix}. \tag{27}$$

As a next step, we multiply Eq. (25) by $\Psi^{(0)}$ from the left and Eq. (27) by Ψ from the left and subtract them from each other. This yields

$$A\frac{d(\psi_e^{(0)}\psi_h - \psi_e\psi_h^{(0)})}{dy} = \delta E_0(k_x)\left(\psi_e^{(0)}(y)\psi_e(y) + \psi_h(y)\psi_h^{(0)}(y)\right). \tag{28}$$

Upon integrating Eq. (28) from $y = 0$ to ∞, we find the analytical expression for $\delta E_0(k_x)$

$$\delta E_0(k_x) = -A\frac{\psi_e^{(0)}(0)\psi_h(0) - \psi_e(0)\psi_h^{(0)}(0)}{\int\limits_0^\infty dy\left(\psi_e^{(0)}(y)\psi_e(y) + \psi_h(y)\psi_h^{(0)}(y)\right)}. \tag{29}$$

The difference between the boundary values $\psi_e(0)$ and $\psi_e^{(0)}(0)$ as well as $\psi_h(0)$ and $\psi_h^{(0)}(0)$ is that the exact wave functions satisfy the boundary condition Eq. (26). The boundary leads to the admixture to $\Psi^{(0)}$ of the "short-range" solution decaying into the bulk as $\exp(-q_0 y)$ and of the "reflected" solution decaying as $\exp(-q_\Delta y)$. The corresponding amplitudes, C_0 and C_Δ, are found from the boundary condition

$$C_0 \begin{pmatrix} -1 \\ 1 \end{pmatrix} + C_\Delta \begin{pmatrix} 1 \\ \frac{A(k_x + q_\Delta)}{m - \Delta + E_0} \end{pmatrix} + \begin{pmatrix} \psi_e^{(0)}(0) \\ \psi_h^{(0)}(0) \end{pmatrix} = 0, \tag{30}$$

which yields

$$C_0 = \frac{-\frac{A(k_x + q_\Delta)}{m - \Delta + E_0}\psi_e^{(0)}(0) + \psi_h^{(0)}(0)}{1 + \frac{A(k_x + q_\Delta)}{m - \Delta + E_0}}, \quad C_\Delta = -\frac{\psi_e^{(0)}(0) + \psi_h^{(0)}(0)}{1 + \frac{A(k_x + q_\Delta)}{m - \Delta + E_0}}. \tag{31}$$

At distance $y \gg l_0$ from the boundary the short-range solution vanishes. Thus, the differences $\psi_h(0) - \psi_h^{(0)}(0)$, and $\psi_e(0) - \psi_e^{(0)}(0)$ are determined only by the reflected solution

$$\begin{pmatrix} \psi_e(0) \\ \psi_h(0) \end{pmatrix} = C_\Delta \begin{pmatrix} 1 \\ \frac{A(k_x + q_\Delta)}{m - \Delta + E_0} \end{pmatrix} + \begin{pmatrix} \psi_e^{(0)}(0) \\ \psi_h^{(0)}(0) \end{pmatrix}. \tag{32}$$

Substituting Eq. (32) into Eq. (29), we express the correction $\delta E_0(k_x)$ via the components of the bare pseudospinor

$$\delta E_0(k_x) = -A\frac{\psi_e^{(0)}(0)\psi_h^{(0)}(0)\left(1 - \frac{k_x + q_\Delta}{k_x - q_\Delta}\right)\left(\frac{1 + \frac{A(k_x - q_\Delta)}{m - \Delta + E_0}}{1 + \frac{A(k_x + q_\Delta)}{m - \Delta + E_0}}\right)}{\int_{-\infty}^{\infty} dy \left[(\psi_e^{(0)}(y))^2 + (\psi_h^{(0)}(y))^2\right]}, \tag{33}$$

where we took into account that $\psi_h^{(0)}(0)/\psi_e^{(0)}(0) = A(k_x - q_\Delta)/(m - \Delta + E_0)$.

We see that the correction is proportional to the product of the bare amplitudes, and thus to $\exp(-2q_\Delta D)$, which is the probability to find an electron at the edge. The result Eq. (33) applies when this probability is small. For this reason we replaced $\psi_e(0)$, $\psi_h(0)$ in the denominator by $\psi_e^{(0)}(0)$, $\psi_h^{(0)}(0)$ and extended the low limit of integration to $-\infty$. To analyze the dependence of the correction on the bare spectrum, $E_0(k_x)$, it is instructive to recast the last bracket into the form

$$\frac{m - \Delta + E_0 + A(k_x - q_\Delta)}{m - \Delta + E_0 + A(k_x + q_\Delta)} = \frac{\left[m - \Delta + E_0 + Ak_x - \sqrt{(m - \Delta)^2 + A^2 k_x^2 - E_0^2}\right]^2}{2(E_0 + Ak_x)(m - \Delta + E_0)}. \tag{34}$$

The above expression illustrates the topological origin of the shift of a nonchiral mode, $E_0(k_x)$. Indeed, the correction Eq. (33) contains a pole corresponding to the dispersion law of the chiral edge mode. This confirms our earlier observation that presence of this mode complicates the formation of nonchiral modes. The shift Eq. (33) tends to reduce the binding energy. Another feature that points at the topological origin of the correction is that it depends on the sign of k_x. This is in contrast to non-perturbed behavior $E_0(k_x)$ which is an even function of k_x. As k_x increases, the parameter q_Δ, which is the characteristics of proximity of $E_0(k_x)$ to the continuous spectrum, becomes much smaller than k_x. Then the second bracket in Eq. (33) is close to 1, while the first bracket falls off as $1/k_x$.

The result Eq. (33) strongly simplifies for small k_x. Then we have

$$\delta E_0(k_x) = -A\frac{2\psi_e^{(0)}(0)\psi_h^{(0)}(0)}{\int_{-\infty}^{\infty} dy \left[(\psi_e^{(0)}(y))^2 + (\psi_h^{(0)}(y))^2\right]}$$
$$\times \left[\frac{(m - \Delta) - \sqrt{(m - \Delta)^2 - E_0^2}}{E_0}\right]. \tag{35}$$

It is the factor in the square brackets that carries information on whether or not the boundary supports the chiral mode. Indeed, if the level, E_0, in the potential $U(y)$ is close to midgap, then this factor diverges for $(m - \Delta) < 0$, while it turns to zero for $(m - \Delta) > 0$. This is because, for $(m - \Delta) < 0$, there is a level $E = 0$ at the boundary from which the level E_0 is repelled. When this level is

absent, the behavior of the shift $\delta E_0 \propto E_0$ is natural. For $E_0 \to 0$ there are equal probabilities to be shifted up or down.

IV. CONCLUDING REMARKS

(i) Presence or absence of chiral modes in QAH effect is decided by the relative sign of $(m - \Delta)$ and parameter B in the Hamiltonian $\hat{h}(\mathbf{k})$, although the parameter B itself does not enter into the dispersion law of the chiral mode. The situation with nonchiral modes is analogous, their dispersion relations do not contain B. Still, these relations depend on whether $(m - \Delta)$ and B have the same sign or opposite signs. Moreover, similarly to chiral mode, nonchiral modes will not exist without the term Bk^2 on the diagonal of the matrix $\hat{h}$. This is because, without the short-range solution $\propto \exp(-q_0 y)$ in Eq. (14), the hard-wall boundary conditions cannot be satisfied.

(ii) Within the standard picture of the QAH transition,[17] it takes place as the gap closes and two chiral modes at the opposite edges merge. Disorder would facilitate this merging and, thus, smear the transition. In this regard, it is instructive to draw an analogy of QAH with conventional quantum Hall transition. This transition is broadened due to the disorder-assisted overlap between the counter-propagating chiral edge modes. This mechanism was appreciated already in the early papers on the quantum Hall effect, see e.g. Refs. 28-31. Quantitatively, scattering by disorder-induced in-gap states effectively enhances the localization radius of the edge modes boosting their overlap. In the present paper we found that extended confinement gives rise to in-gap nonchiral modes. This suggests that chiral edge modes can "communicate" with each other using nonchiral modes, which are less localized, as virtual intermediate states.[28–31] This

is how the extended confinement may cause the smearing of the QAH transition.

(iii) Our other finding is that, while nonchiral modes are present for both signs of $(m - \Delta)$, their formation is much less likely for $(m - \Delta) < 0$. This can be interpreted as follows. The pseudospinor corresponding to nonchiral mode should be orthogonal to the chiral mode, if it is present. Thus the formation of nonchiral mode is impeded for "topological" sign of $(m - \Delta)$.

(iv) In Ref. 32 it was assumed that the boundary of the system is planar, and the generalized, compared to hard wall, version of the boundary conditions was employed. It was demonstrated that variation of parameters in the boundary condition can lead to disappearance of the chiral mode form the gap, but nonchiral modes do not emerge upon this variation.

(v) It is straightforward to generalize our results for rectangular step to arbitrary profile of the step. Essentially, the decay constant κ defined by Eq. (13) becomes the function of coordinate. Qualitative conclusions do not change.

(vi) The probable microscopic origin of the extended confinement is a conventional band bending at the interface. For the material Bi_2Se_3 this bending was studied experimentally in Ref. 34. According to this paper, the extension of the bending region is about $200\mathring{A}$, while bending magnitude is about 0.2eV. These quantities should be viewed as estimates for our d and U_0.

V. ACKNOWLEDGEMENTS

[1] J. G. Checkelsky, J. Ye, Y. Onose, Y. Iwasa, and Y. Tokura, Nat. Phys. **8**, 729 (2012).

[2] C.-Z. Chang, J. Zhang, M. Liu, Z. Zhang, X. Feng, K. Li, L.-L. Wang, X. Chen, X. Dai, Z. Fang, X.-L. Qi, S.-C. Zhang, Y. Wang, K. He, X.-C. Ma, and Q.-K. Xue, Adv. Mater. **25**, 1065 (2013).

[3] X. Kou, M. Lang, Y. Fan, Y. Jiang, T. Nie, J. Zhang, W. Jiang, Y. Wang, Y. Yao, L. He, and K. L. Wang, ACS Nano **7**, 9205 (2013).

[4] C.-Z. Chang, J. Zhang, X. Feng, J. Shen, Z. Zhang, M. Guo, K. Li, Y. Ou, P. Wei, L.-L. Wang, Z.-Q. Ji, Y. Feng, S. Ji, X. Chen, J. Jia, X. Dai, Z. Fang, S.-C. Zhang, K. He, Y. Wang, L. Lu, X.-C. Ma, and Q.-K. Xue, Science **340**, 167 (2013).

[5] J. G. Checkelsky, R. Yoshimi, A. Tsukazaki, K. S. Takahashi, Y. Kozuka, J. Falson, M. Kawasaki, and Y. Tokura, Nat. Phys. **10**, 731 (2014).

[6] X. Kou, S.-T. Guo, Y. Fan, L. Pan, M. Lang, Y. Jiang, Q.

Shao, T. Nie, K. Murata, J. Tang, Y. Wang, L. He, T.-K. Lee, W.-L. Lee, and K. L. Wang, Phys. Rev. Lett. **113**, 137201 (2014).

[7] C.-Z. Chang, W. Zhao, D. Y. Kim, H. Zhang, B. A. Assaf, D. Heiman, S.-C. Zhang, C. Liu, M. H. W. Chan. and J. S. Moodera, Nat. Mater. **14**, 473 (2015).

[8] A. Kandala, A. Richardella, S. Kempinger, C.-X. Liu, N. Samarth, Nat. Commun. **6**, 7434 (2015).

[9] M. Mogi, R. Yoshimi, A. Tsukazaki, K. Yasuda, Y. Kozuka, K. S. Takahashi, M. Kawasaki, and Y. Tokura, Appl. Phys. Lett. **107**, 182401 (2015).

[10] X. Kou, L. Pan, J. Wang, Y. Fan, E. S. Choi, W.-L. Lee, T. Nie, K. Murata, Q. Shao, S.-C. Zhang, and K. L. Wang, Nat. Commun. **6**, 8474 (2015).

[11] A. J. Bestwick, E. J. Fox, X. Kou, L. Pan, K. L. Wang, and D. Goldhaber-Gordon, Phys. Rev. Lett. **114**, 187201 (2015).

[12] C.-Z. Chang, W. Zhao, D. Y. Kim, H. Zhang, B. A. Assaf,

D. Heiman, S.-C. Zhang, C. Liu, M. H. W. Chan, and J. S. Moodera, Nat. Mater. **14**, 473 (2015).

[13] C.-Z. Chang, W. Zhao, D. Y. Kim, P. Wei, J. K. Jain, C. Liu, M. H. W. Chan, and J. S. Moodera, Phys. Rev. Lett. **115**, 057206 (2015).

[14] S. Grauer, S. Schreyeck, M. Winnerlein, K. Brunner, C. Gould, and L. W. Molenkamp, Phys. Rev. B **92**, 201304(R) (2015).

[15] E. O. Lachman, A. F. Young, A. Richardella, J. Cuppens, H. R. Naren, Y. Anahory, A. Y. Meltzer, A. Kandala, S. Kempinger, Y. Myasoedov, M. E. Huber, N. Samarth, and E. Zeldov, Sci. Adv. **1**, e1500740 (2015).

[16] X.-L. Qi, Y.-S. Wu, and S.-C. Zhang, Phys. Rev. B **74**, 085308 (2006).

[17] C.-X. Liu , X.-L. Qi, X. Dai, Z. Fang, and S.-C. Zhang, Phys. Rev. Lett. **101**, 146802 (2008).

[18] J. Wang, B. Lian, H. Zhang, and S.-C. Zhang, Phys. Rev. Lett. **111**, 086803 (2013).

[19] E. B. Sonin, Phys. Rev. B **82**, 113307 (2010).

[20] B. Scharf, A. Matos-Abiague, and J. Fabian, Phys. Rev. B **86**, 075418 (2012).

[21] A. M. Lunde and G. Platero, Phys. Rev. B **88**, 115411 (2013).

[22] M. V. Durnev and S. A. Tarasenko, Phys. Rev. B **93**, 075434 (2016),

[23] B. A. Bernevig, T. L. Hughes, and S.-C. Zhang, Science **314**, 1757 (2006).

[24] Following C.-X. Liu, S.-C. Zhang, and X.-L. Qi, arXiv:1508.07106, we assumed that the absolute values of diagonal components of $\hat{h}_{\mathrm{exch}}$ are equal to each other. In fact, the band inversion requires only that the signs of these components within one block are opposite.[17] Still the form Eq. (2) is not a loss of generality. Indeed, if the sum of these components is nonzero, it causes an overall shift of the spectrum.

[25] To estimate the length l_0 we take the experimental value $B = 60\mathrm{eV}\cdot\mathring{A}^2$ from Ref. 33 and the value $A = 3\mathrm{eV}\cdot\mathring{A}$ from Ref. 17. This yields $l_0 = B/A = 20\mathring{A}$, which is only 3 times bigger than the distance between the magnetic dopants in experiment as well as the thickness of the layer where the surface reconstruction[35] takes place. On the other hand, for the gap $\sim 10\mathrm{meV}$ the length l_Δ is $\sim 300\mathring{A}$, i.e. it is much bigger.

[26] In fact, Eq. (22) has solutions for arbitrary positive n. However, only finite number of corresponding dispersion curves lie inside the gap. The curves, corresponding to large n, lie in the domain $\mathcal{E} < -1$ and have their staring points at the bulk spectrum.

[27] M. I. Dyakonov and A. V. Khaetskii, JETP Lett. **33**, 110 (1981) [Pisma Zh. Eksp. Teor. Fiz. **33**, 115 (1981)].

[28] J. K. Jain and S. A. Kivelson, Phys. Rev. Lett. **60**, 1542 (1988).

[29] T. Martin and S. Feng, Phys. Rev. Lett. **64**, 1971 (1990).

[30] J. Hajdu, M. E. Raikh, and T. V. Shahbazyan, Phys. Rev. B **50**, 17625 (1994).

[31] M. M. Fogler, A. Yu. Dobin, and B. I. Shklovskii, Phys. Rev. B **57**, 4614 (1998).

[32] V. V. Enaldiev, I. V. Zagorodnev, and V. A. Volkov, Pisma Zh. Eksp. Teor. Fiz. **101**, 94 (2015) [JETP Lett. **101**, 89 (2015)].

[33] H. Zhang, C. Liu, X. Qi, X. Dai, Z. Fang, and S. Zhang, Nat. Phys. **5**, 438 (2009).

[34] C. E. ViolBarbosa, C. Shekhar, B. Yan, S. Ouardi, E. Ikenaga, G. H. Fecher, and C. Felser, Phys. Rev. B **88**, 195128 (2013).

[35] T. M. Edmonds, J. T. Hellerstedt, A. Tadich, A. Schenk, K. M. ODonnell, J. Tosado, N. P. Butch, P. Syers, J. Paglione, and M. S. Fuhrer, J. Phys. Chem. C **118**, 20413 (2014).